Mutant SPTLC1 dominantly inhibits serine palmitoyltransferase activity *in vivo* and confers an age-dependent neuropathy

Alexander McCampbell[1],*, David Truong[1], Daniel C. Broom[3], Andrew Allchorne[3], Ken Gable[5], Roy G. Cutler[7], Mark P. Mattson[7], Clifford J. Woolf[3], Matthew P. Frosch[2,4], Jeffrey M. Harmon[6], Teresa M. Dunn[5] and Robert H. Brown, Jr[1]

[1]Day Laboratory for Neuromuscular Research, [2]Alzheimer's Research Unit, Mass General Institute for Neurodegenerative Disease, [3]Neural Plasticity Research Group, Department of Anesthesia and Critical Care, [4]C.S. Kubik Laboratory for Neuropathology, Department of Pathology, Massachusetts General Hospital and Harvard Medical School, Charlestown, MA 02129, USA, [5]Department of Biochemistry and Molecular Biology, [6]Department of Pharmacology, Uniformed Services University of the Health Sciences, Bethesda, MD 20184-4799, USA and [7]Laboratory of Neurosciences, National Institute on Ageing Intramural Research Program, Baltimore, MD 21224, USA

Mutations in enzymes involved in sphingolipid metabolism and trafficking cause a variety of neurological disorders, but details of the molecular pathophysiology remain obscure. *SPTLC1* encodes one subunit of serine palmitoyltransferase (SPT), the rate-limiting enzyme in sphingolipid synthesis. Mutations in *SPTLC1* cause hereditary sensory and autonomic neuropathy (type I) (HSAN1), an adult onset, autosomal dominant neuropathy. HSAN1 patients have reduced SPT activity. Expression of mutant SPTLC1 in yeast and mammalian cell cultures dominantly inhibits SPT activity. We created transgenic mouse lines that ubiquitously overexpress either wild-type (SPTLC1^WT) or mutant SPTLC1 (SPTLC1^C133W). We report here that SPTLC1^C133W mice develop age-dependent weight loss and mild sensory and motor impairments. Aged SPTLC1^C133W mice lose large myelinated axons in the ventral root of the spinal cord and demonstrate myelin thinning. There is also a loss of large myelinated axons in the dorsal roots, although the unmyelinated fibers are preserved. In the dorsal root ganglia, IB4 staining is diminished, whereas expression of the injury-induced transcription factor ATF3 is increased. These mice represent a novel mouse model of peripheral neuropathy and confirm the link between mutant SPT and neuronal dysfunction.

INTRODUCTION

Hereditary sensory and autonomic neuropathy (type I) (HSAN1) is an adult onset, autosomal dominant neuropathy, which is the most common hereditary disorder primarily affecting peripheral sensory neurons. The clinical presentation varies, but unifying characteristics include profound sensory and motor loss associated with ulcerative mutilations, weakness and hyporeflexia (1). Distal muscle wasting is frequent, as are diminished autonomic responses. Histological examination reveals decrease in all fiber types in distal axons, including both unmyelinated and myelinated fibers.

Electrophysiological data suggested a more profound loss of unmyelinated fibers (2). The most severely affected neuronal population is the dorsal root ganglia (DRG) of the lumbosacral region. Within the DRG, there is a preferential loss of small cells (3,4).

The genetic basis for HSAN1 has been identified as missense mutations in the *SPTLC1* gene (5,6). *SPTLC1* is highly conserved within eukaryotic organisms, and both *SPTLC1* and its heterodimeric partner, *SPTLC2*, are members of the α-oxoamine synthase family (7). The *SPTLC1* gene encodes a 473 amino acid protein, a subunit of the enzyme serine palmitoyltransferase (SPT). SPT catalyzes the

---

*To whom correspondence should be addressed. Tel: +1 6177245334; Fax: +1 6177248543; Email: amccampbell@partners.org

condensation of serine and palmitoyl-CoA to generate 3-ketosphinganine, the rate-limiting step in *de novo* sphingolipid biosynthesis. 3-Ketosphinganine is further metabolized to sphingosine, a precursor to ceramide. Ceramides are important in intracellular signaling, although their precise role is controversial. They may act as traditional second messengers, analogous to diacylglycerol (DAG) (8,9), and it has also been proposed that they are involved in the formation of lipid rafts that organize proteins within microdomains of the membrane (10,11).

To date, four mutations in *SPTLC1* have been found in HSAN1 patients (5,6,12). Three of these mutations, C133Y, C133W and V144D, result in a protein that can heterodimerize with SPTLC2, but the resulting complex lacks SPT activity (7,13). The fourth mutation, G387A, was identified in twin sisters diagnosed with HSAN1. The impact of this mutation on SPT activity is currently unknown. Despite extensive sequencing, no mutation in *SPTLC2* has been identified in HSAN1 patients (14).

The autosomal dominant inheritance pattern, age of onset and type of mutation are most consistent with either of two hypotheses for the pathogenesis of HSAN1, corresponding to either loss- or gain-of-function. One is that peripheral sensory and motor neurons (and particularly small fiber sensory neurons) are sensitive to perturbations of sphingolipid metabolism caused by mutation-induced reduction in SPT enzyme activity. This hypothesis is consistent with the reduced SPT activity in HSAN1 patients and *in vitro* data demonstrating that each of the mutations examined to date decreases SPT activity (7,13). Although one might anticipate a concomitant change in cellular lipid compositions, the data have been conflicting. Different investigators have reported increases in glucosylceramide synthesis (5), decreases in ceramide and sphingomyelin synthesis (13) and no change in lipid composition within patient samples (15). The source of variability in the results is not clear, although it may be related to the limited availability of patient samples.

Alternatively, the mutations may confer one or more toxic properties on SPTLC1. In other dominantly inherited neurodegenerative diseases, neuronal dysfunction and death are a consequence of misfolding of the mutant protein and aberrant protein–protein interactions (16). Regardless of whether *SPTLC1* mutations diminish SPT activity or render SPT toxic through adverse protein behavior, it is clear that sphingolipids are critical to neuronal function and mutations that perturb their synthesis, trafficking and degradation can be neurotoxic. Analysis of the molecular pathobiology of mutant SPT in HSAN1 might therefore provide important insights into the function of these critical lipids and the pathogenesis of the disease.

As a first step in differentiating between these hypotheses, we sought to determine whether overexpression of an HSAN1-causing allele in mice can re-create important aspects of the HSAN1 pathology. To do this, we expressed the mutant SPTLC1 protein at superphysiological levels to increase the chances of inducing a robust phenotype. Transgenic mouse lines were established, in which either wild-type or mutant SPTLC1 was expressed from the chicken beta actin promoter. We report here that mice expressing mutant SPTLC1 have impaired SPT activity and that by 10 months of age,

they develop mild sensory and motor deficits. Furthermore, there is peripheral axonal myelin thinning and loss of visceral innervation along with indications of neuronal stress within the dorsal root ganglia. These data indicate that mutant SPTLC1 can act as a dominant negative inhibitor of SPT activity and induce a progressive neurological impairment involving analogous neuronal populations affected in humans with HSAN1. Additional mouse lines will be necessary to conclusively distinguish between the biochemical and toxic protein hypotheses.

RESULTS

We created transgenic mice expressing either wild-type *SPTLC1* or a mutant form of *SPTLC1*. We chose the C133W mutation because it is the most common HSAN1 mutation and two of the four known mutations alter amino acid 133 (5,6). Results in culture systems have shown that SPTLC1^{C133W} is a dominant negative inhibitor of SPT (7). To achieve robust and ubiquitous expression of the transgene, we used the chicken beta-actin promoter with CMV enhancer elements (Fig. 1A). *Cricetulus griseus* (Chinese hamster) *SPTLC1* cDNA sequence was used. It encodes a protein with 96% amino acid to identify the murine protein. The hamster cDNA was selected because of our extensive experience with the hamster protein and its demonstrated ability to complement SPT activity in CHO and yeast cells lacking SPTLC1 (7,17). Finally, we used a C-terminal hemagglutinin (HA) epitope tag to distinguish between endogenous SPTLC1 and the transgene.

Prior to the generation of these mouse lines, we confirmed expression and function of the construct by transient transfection into CHO-K1 cells (Fig. 1B). Expression of SPTLC1 or SPTLC1-HA alone did not result in increased SPT activity (lanes 2 and 4). This result suggests that SPTLC2 is limiting in these cells. Consistent with this, coexpression of either construct with SPTLC2 resulted in a significant increase in SPT activity (lanes 3 and 5). Introduction of the C133W mutation conferred the anticipated dominant negative property (lanes 6 and 8), and this dominant negative effect was not altered by the HA tag. In addition, the HA tag conferred the expected decreased mobility by SDS–PAGE. These results indicate that the HA tag does not alter normal SPTLC1 function and that the C133W mutation confers the expected dominant negative activity.

Initial characterization of mice

The SPTLC1-HA and SPTLC1-C133W-HA constructs were used to generate transgenic mouse lines, designated SPTLC1^{WT} and SPTLC1^{C133W}, respectively. After genotyping and confirmation of germline transmission, we performed western blot analyses on tail snips and quantified the amount of transgene relative to endogenous SPTLC1 expression levels. SPTLC1^{WT} expressing mice (6B, 6F and 6H) demonstrated transgene expression at 3.3, 4.7 and 5.6 times endogenous SPTLC1 levels, respectively. Transgene expression in SPTLC1^{C133W} lines 8B, 8E and 8F were 0.7, 3.9 and 0.4 times endogenous levels. In general, the SPTLC1^{C133W}
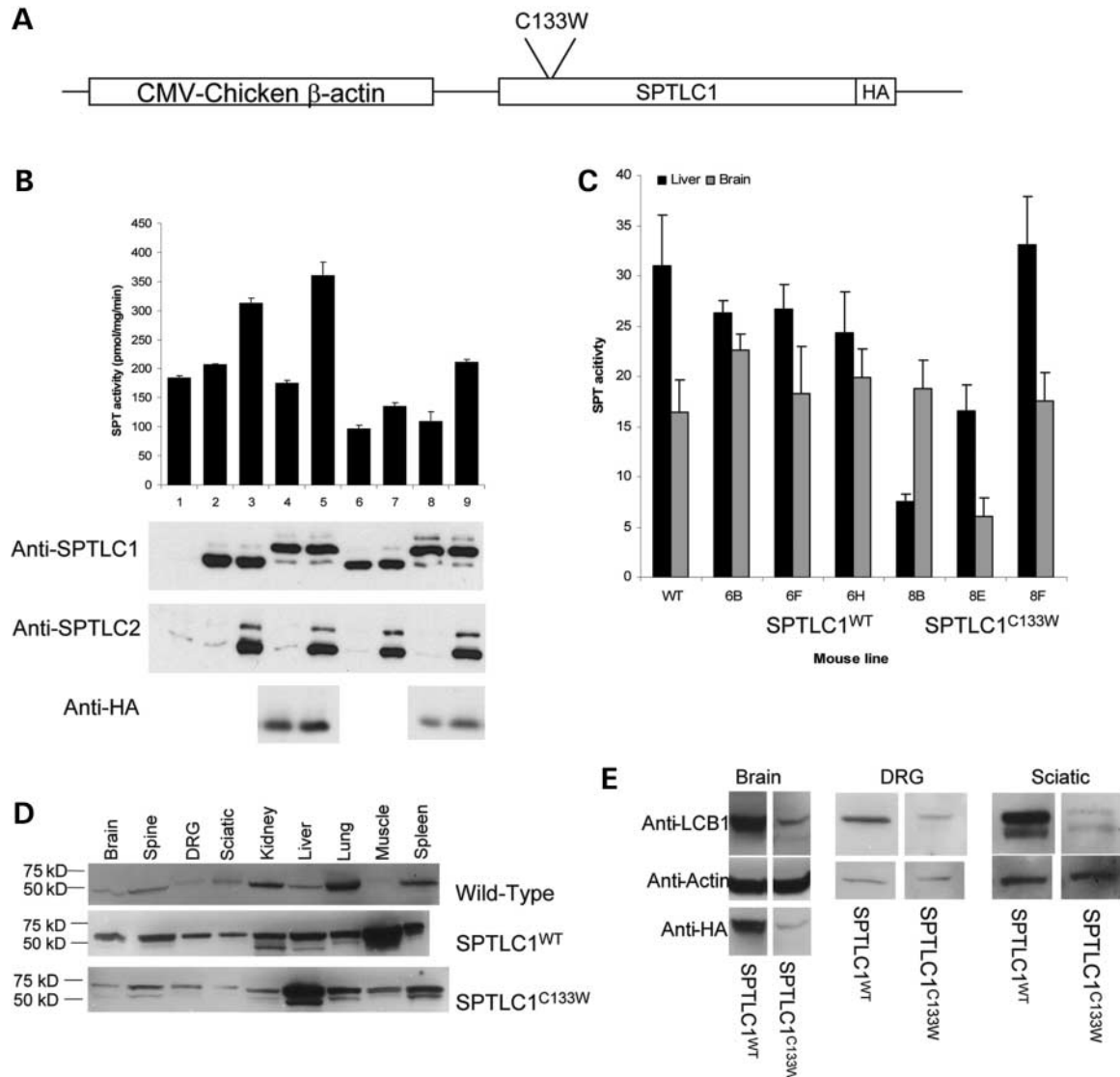
Figure 1. Expression of normal or dominant negative SPTLC1 in mice. (**A**) A series of four constructs were created using the CHO cDNA for the SPTLC1 gene. Both wild-type (SPTLC1) and mutant (C133W) constructs were made. In addition, an HA tag was introduced to facilitate identification of the transgene. (**B**) Transient transfection of CHO cells with C133W constructs inhibits SPT activity. Upper panel indicates SPT activity (pmol/mg protein/min), whereas the lower panels are western blot analysis of microsomes from the same cells. *Lane 1*: Untransfected cells; *Lane 2*: SPTLC1; *Lane 3:* SPTLC1 and SPTLC2; *Lane 4*: SPTLC1-HA; *Lane 5*: SPTLC1-HA and SPTLC2; *Lane 6*: C133W; *Lane 7*: C133W and SPTLC2; *Lane 8*: C133W-HA; *Lane 9*: C133W-HA and SPTLC2. Blots were probed with antibodies to SPTLC1, SPTLC2 or HA. (**C**) SPT activity is decreased in the liver and CNS of mice expressing C133W. SPT activity in purified microsomes from tissues of three separate SPLC1^{WT} and SPTLC1^{C133W} expressing lines shown along with samples from wild-type mice ($n = 5$, bars indicate standard error). (**D**) SPTLC1^{WT} (6F) and SPTLC1^{C133W} (8E) are overexpressed in a variety of tissues. Microsomes from wild-type, SPTLC1^{WT} and SPTLC1^{C133W} mice were probed with anti-LCB1. The lower band corresponds to endogenous SPTLC1 and the upper to the HA-tagged transgene. (**E**) The transgene is expressed in multiple regions of the CNS. Homogenates from brain, dorsal root ganglia and sciatic nerve were probed with anti-LCB1 and anti-HA. Protein loading was normalized to anti-actin staining.

expression was lower than SPTLC1^{WT}. This may reflect decreased protein stability in the mutant, as quantitative RT–PCR analysis revealed that transcript levels were comparable (data not shown). The high, medium and low expressing lines were selected for the analysis of SPT activity in isolated microsomes derived from the brain and liver. In wild-type mice, SPT activity in the brain was roughly 50% of that found in liver (Fig. 1C). This correlates with expression levels of SPTLC1 and SPTLC2 (data not shown).

The SPTLC1^{WT} expressing mice all had near-normal levels of SPT activity in the liver and brain. As in the cell culture experiments, we were unable to achieve superphysiological levels of SPT activity by overexpression of SPTLC1; we speculate that this would require concomitant overexpression of *SPTLC2*. Endogenous SPTLC1 levels were not altered by overexpression of the wild-type transgene (data not shown). This is consistent with yeast and mammalian culture data suggesting that SPTLC1 is not the limiting factor in SPT activity (7). The 8E line, which expressed the highest level

of transgene, had the lowest SPT activity in the brain ($P < 0.05$) and decreased SPT activity in the liver ($P < 0.05$). The 8B line, the mid-range expresser, had significantly decreased SPT activity in the liver ($P < 0.05$); however, the SPT activity in brain-derived microsomes was comparable to wild-type. The 8B line did not have increased expression in the liver when compared with 8E, indicating a possible separation of protein expression and SPT inhibition. In the 8F line, which expresses only a very low level of the transgene, SPT activity was unchanged from wild-type mice. SPT activity was unchanged in the spinal cord of either the SPTLC1^{WT} or the SPTLC1^{C133W} mice. These results are consistent with previous reports that the C133W mutant acts as a dominant negative inhibitor of SPT and that mutant SPTLC1 can repress SPT activity in two different tissues in mice. Higher mutant SPTLC1 expression generally corresponds with greater SPT repression, although the association is not perfect.

Western blot analysis confirmed the ubiquitous expression of the transgenes in both the SPTLC1^{WT} (6F) and SPTLC1^{C133W} (8E) lines (Fig. 1D). As the transgene has an HA tag, the anti-LCB1 antibody detects a doublet, with the lower band corresponding to the endogenous LCB1 and the upper band to the tagged transgene. The transgene-encoded proteins were readily detectable by either anti-SPTLC1 (Fig. 1D) or anti-HA antibodies (data not shown). Expression of endogenous SPTLC1 varies across tissues, but correlates with microarray data for transcript distribution (18). Expression of the transgene, though consistently higher than endogenous SPTLC1 expression, also varied across tissues. In the kidney, where SPTLC2 expression is greatest, the transgene from both the SPTLC1^{WT} and SPTLC1^{C133W} mice migrated as a high-molecular weight aggregate (data not shown). The initial grouping of mice into high, medium and low expressing on the basis of transgene expression in tail snips was confirmed by western blot analysis of brain and liver homogenates (data not shown). In addition to the brain, the transgene was present in other neural tissues, including dorsal root ganglia (DRG) and the sciatic nerve (Fig. 1E). As noted earlier, expression of SPTLC1-C133W-HA was consistently lower than that of SPTLC1-HA when compared with actin loading. With the exception of the sciatic tissue, the transgene expression was above endogenous protein levels.

To further assess the biochemical consequences of mutant SPT expression, we harvested the spinal cords from wild-type, SPTLC1^{WT} and SPTLC1^{C133W} mice and quantified ceramide, sphingomyelin, cholesterol and phospholipids levels by mass spectroscopy. Tissues were collected at two months of age, prior to detected CNS pathology (see what follows). There was no change in total ceramide, total sphingomyelin, cholesterol or the phospholipids (Fig. 2A and B; data not shown). The lack of change in lipid composition is consistent with the findings of Dedov *et al.* (15). We next examined the ceramide and sphingomyelin pools for changes in fatty acid incorporation. The sphingomyelin pool did not change significantly in its representation of fatty acid chain lengths. In contrast, there is a selective increase in ceramide species with C16:0 and C18:0 fatty acids (Fig. 2C and D; $P < 0.05$) in the SPTLC1^{C133W} mice. This shift may reflect a change in the available pool of fatty acids resulting from decreased utilization of palmitic acid by SPT.

Behavior

For most of our subsequent analyses, we compared mid-range SPTLC1^{WT} line (6F) with the highest expressing mutant line SPTLC1^{C133W} (8E), as these lines had the most comparable levels of transgene expression. Unless explicitly mentioned, all subsequent data are derived from these two lines. The SPTLC1^{C133W} mice were 15–20% smaller than their wild-type littermates (Fig. 3A) ($P < 0.05$). The size decrease was present by 1 month and persisted until the mice were sacrificed at 10 months. The cause of their smaller mass is unknown, although it may be related to their autonomic deficits or pancreatic degeneration (see below). Unlike HSAN1 patients, these mice did not display ulcerative mutilations; nor was there loss of digits through self-induced mutilation. Their gait was grossly normal. However, when lifted by the tail, they exhibited unusually rapid hind leg kicking and distinctive extension of the hind legs parallel to the tail (Supplementary material). Blinded scoring of videos by observers familiar with leg flexion analysis in mice corroborated this significant increase in leg kicking activity (Fig. 3B) ($P < 0.05$, Mann–Whitney). The hyperkinesis manifested at 6–8 months of age and persisted without obvious progression. Despite this hind limb hyperkinesis, other measures of motor performance were normal up to 10 months of age. There was no difference in rotorod performance on an accelerating rod paradigm at 3–5 or 8–10 months of age (data not shown).

To assess changes in pain sensitivity, we measured response thresholds to noxious mechanical and temperature stimuli. At 3–5 months of age, there was no difference between the groups in any of the sensory assays (data not shown). At 8–10 months, the SPTCL1^{C133W} mice responded no differently than wild-type or SPTLC1^{WT} mice to Von Frey, pinprick or acetone (cold) stimuli (Fig. 3C). However, the older SPTLC1^{C133W} mice were significantly more sensitive to thermal pain. The dissociation between thermal and mechanical thresholds is interesting, as thermal hyperalgesia can occur in the initial stages of HSAN1.

General histology

A general autopsy was performed on one female and two male mice at 10 months of age. The two most striking, non-CNS changes were the presence of abnormal spermatogenesis and degeneration of the exocrine pancreas (Fig. 4A). As oogenesis appeared normal, the abnormal sperm production may account for the decreased fertility observed in our colony. In the pancreas, the islets appeared well preserved, whereas the acinar cells were largely replaced by fatty infiltrates. In normal BL6C3H mice, exocrine pancreatic degeneration is observed in roughly 1–2% of mice by 1 year of age, although it is of unknown etiology (19). This is distinct from the time course of pancreatic degeneration in our SPTLC1^{C133W} mice, which was present as early as 4 months of age. To assess the status of neuronal innervation of the pancreas, we performed immunostaining with anti-PGP9.5 antibody, which stains ubiquitin c-terminal esterase L1 and thereby efficiently identifies neurites (20,21). Anti-PGP9.5 labels both ganglionic neurons around the islets and neurites (Fig. 4B) in the SPTLC1^{WT}
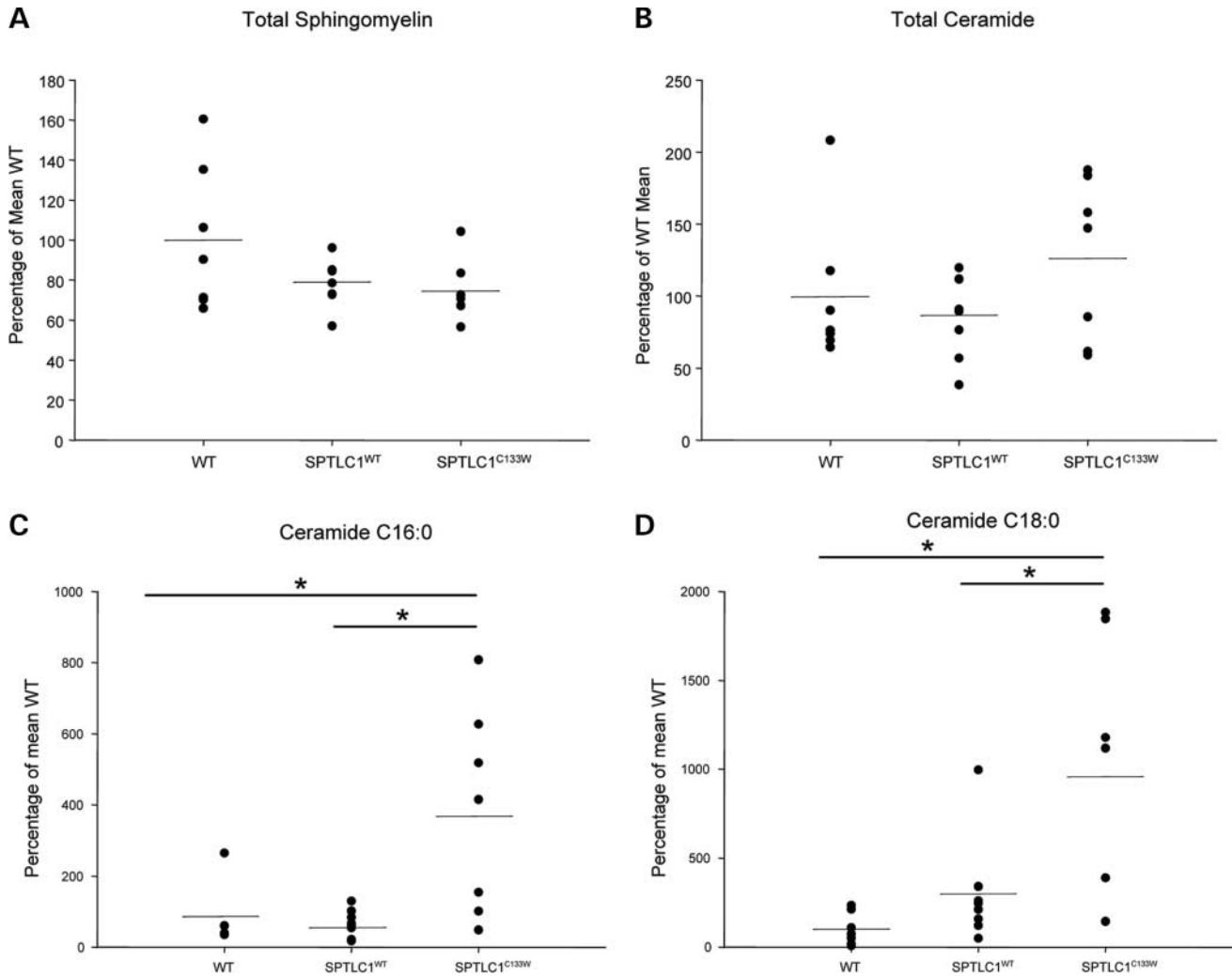
Figure 2. Selective increase in C16:0 and C18:0 ceramide in the CNS of young SPTLC1[C133W] mice. (**A**) Total sphingomyelin and (**B**) total ceramide levels are unchanged among wild-type, SPTLC1[WT] and SPTLC[C133W] mice. Data are expressed relative to the mean total ceramide levels in the wild-type samples. (**C**) C16:0 and (**D**) C18:0 ceramide are selectively increased in SPTLC1[C133W] mice compared with littermate controls or SPTLC1[WT] mice ($P < 0.05$). All other ceramide species and sphinogmyelin species were not significantly different.

tissue. In the SPTLC1[C133W] pancreas, staining is preserved in the neuronal cell bodies. Neuritic staining is absent even in those regions with intact acinar cells.

Smooth muscle motility is regulated by the autonomic nervous system. In the SPTLC1[C133W] mice, smooth muscle motility appeared to be abnormal, because these mice showed decreased fecal production concomitantly with the decreased body mass. Wild-type mice produced significantly more fecal material during 18 h than the SPTLC1[C133W] mice (400 ± 108 versus 243 ± 69 mg; $P < 0.05$). A more direct assessment of gastrointestinal muscle activity is the gastrointestinal transit assay (22), which monitors the transit time of a bolus of blue dextran-labeled flour placed into the stomach by oral gavage. After 15 min, the distance traveled by the blue dye was significantly lower in the SPTLC1[C133W] mice than in littermate controls or SPTLC1[WT] mice ($P < 0.05$) (Fig. 4C). This provides a direct demonstration that smooth muscle motility is decreased in these mice; this may account in part for their decreased body mass. As the smooth muscle of the intestinal wall was not different between the SPTLC1[WT] and SPTLC1[C133W] mice, these data suggest that the difference can be attributed to an altered neuronal innervation of the gastrointestinal system.

CNS morphometry

As examined by histological studies with hemotoxylin and eosin (H&E) staining, there were no major changes in the CNS of the SPTLC1[C133W] mice. Luxol fast blue and silver staining of longitudinal sections of peripheral nerves was consistent with an axonopathy (data not shown), a finding that was confirmed by quantitative assessment of ventral and dorsal roots of the lumbar region of the spinal cord (Fig. 5). Quantitative morphometry applied to electron micrographs revealed a loss of large caliber axons in the SPTLC1[C133W] mice in both the ventral and dorsal roots (Fig. 5B) ($P < 0.05$).
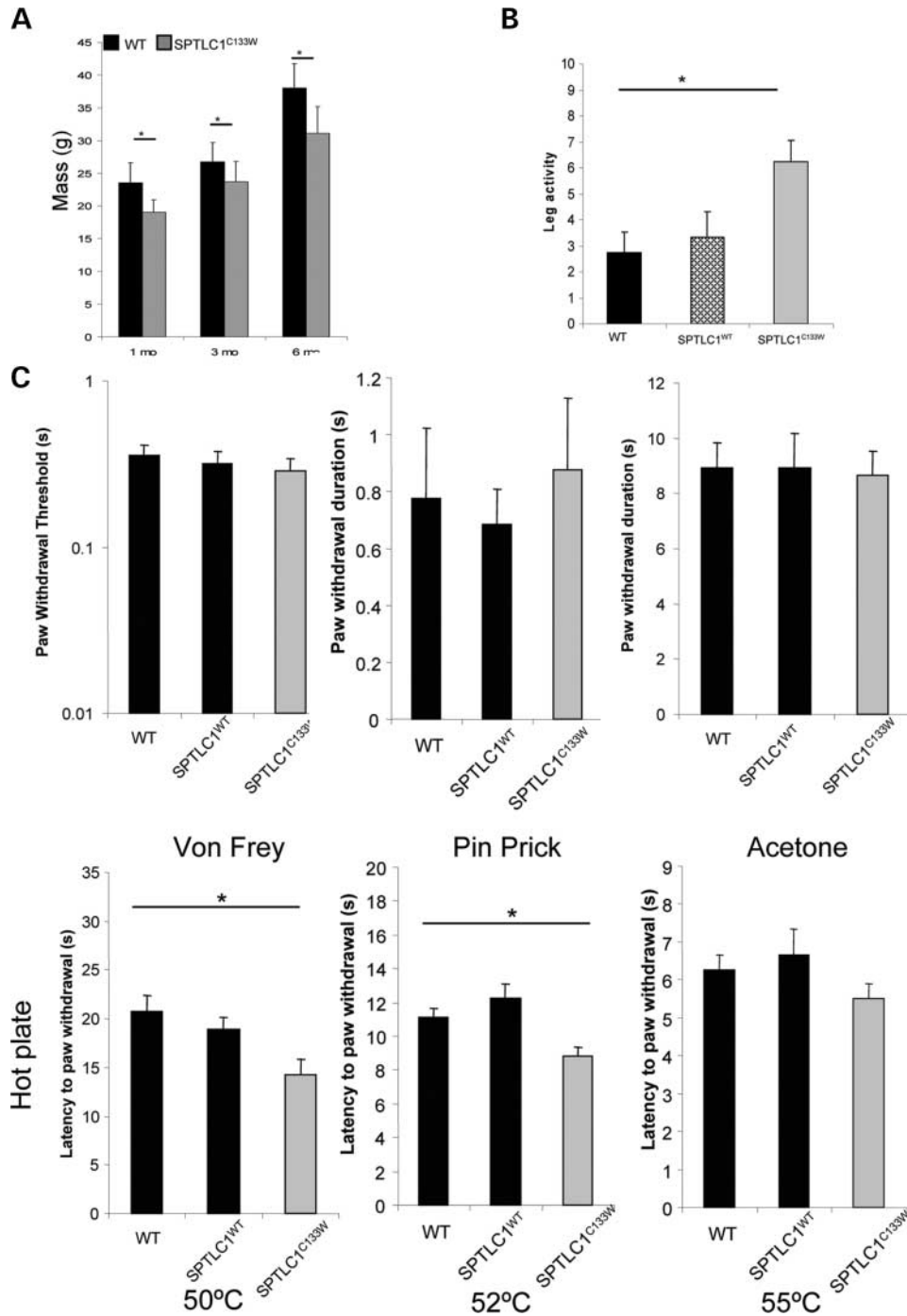
Figure 3. SPTLC1[C133W] mice acquire mild motor and sensory impairments with age. (**A**) SPTLC1[C133W] mice are smaller than wild-type mice, starting at 1 month of age (*$P < 0.05$). (**B**) SPTLC1[C133W] mice have hyperkinetic leg response during tail lift exam (*$P < 0.05$, Mann–Whitney). (**C**) Thermal hyperalgesia in mature SPTLC1[C133W] mice. Sensory performance was evaluated in 10-month-oldwild-type, SPTLC1[WT] and SPTLC1[C133W] mice with Von Frey hair, pin prick assay, acetone exposure and hot plate test. SPTLC1[C133W] mice were significantly quicker to react in the hot plate tests at 50 and 52°C ($P < 0.05$).

Furthermore, there was a reduction in the cross-sectional area of the lumbar ventral roots in the SPTLC1[C133W] mice (Fig. 5C) ($P < 0.05$). These changes in axon number and size were accompanied by myelin thinning in the large axons of the ventral roots in SPTLC1[C133W] mice (Fig. 5A). To quantify this, we calculated the *g*-ratio (the ratio of axon

diameter to overall fiber diameter) for the axons. In the SPTLC1[C133W] mice, there was a significant increase in the ventral root *g*-ratio, which appears to primarily affect the largest fibers (Fig. 5C) ($P < 0.05$). This increase in the ventral root *g*-ratio reflects myelin thinning, evident in Figure 5A (lower right panel). There was no difference in
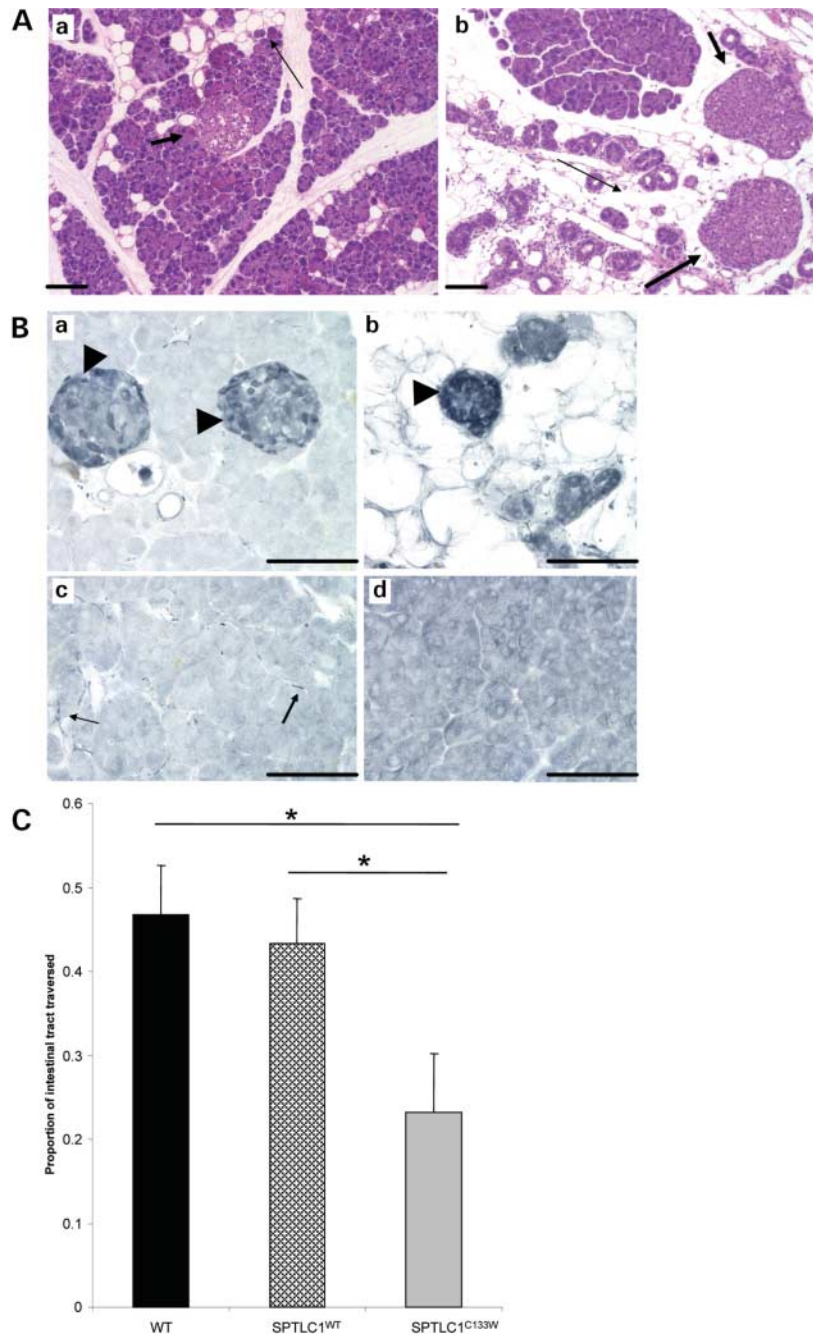
Figure 4. Degeneration of pancreatic exocrine cells in 10-month-old SPTLC1^{C133W} mice is coupled with neurite loss and decreased smooth muscle motility. (**A**) H&E stain of pancreas from SPTLC1 (a) and SPTLC1^{C133W} (b) mice. Thin arrows indicate exocrine cell populations which have been replaced by fatty infiltrates. Thick arrows indicate islets of Langerhan (bar = 100 μm). (**B**) Loss of pancreatic neurites in SPTLC1^{C133W} mice. PGP9.5 staining labels ganglionic neurons (arrow heads) surrounding the islet cells in SPTLC1^{WT} (a) and SPTLC1^{C133W} (b) sections. Although neurites (arrows) can be detected in SPTLC1^{WT} pancreas (**C**), they are absent in the SPTLC1^{C133W} pancreas (d) (bar = 250 μm). (**D**) SPTLC1^{C133W} mice have decreased smooth muscle motility as assessed by the gastrointestinal transit assay. The proportion of the GI tract traversed by a blue dextran-flour bolus was measured in wild-type, SPTLC1^{WT} and SPTLC1^{C133W} mice. The dye front migrates significantly further in the wild-type and SPTLC1^{WT} mice than in the SPTLC1^{C133W} mice (*$P < 0.05$).

the dorsal root *g*-ratio, and the SPTLC1^{WT} mice were normal in both tissue sets. We also examined the unmyelinated fibers in the dorsal roots (Fig. 6). There was no change in the unmyelinated fiber density in the dorsal roots, suggesting that the proximal portions of the C-fibers are intact.

We examined the spinal cord for signs of active axonal degeneration and reactive changes. Immunostaining with markers for activated microglia (CD68) and reactive astrocytes (GFAP) was unremarkable (data not shown). SMI32 staining, which labels non-phosphorylated neurofilament
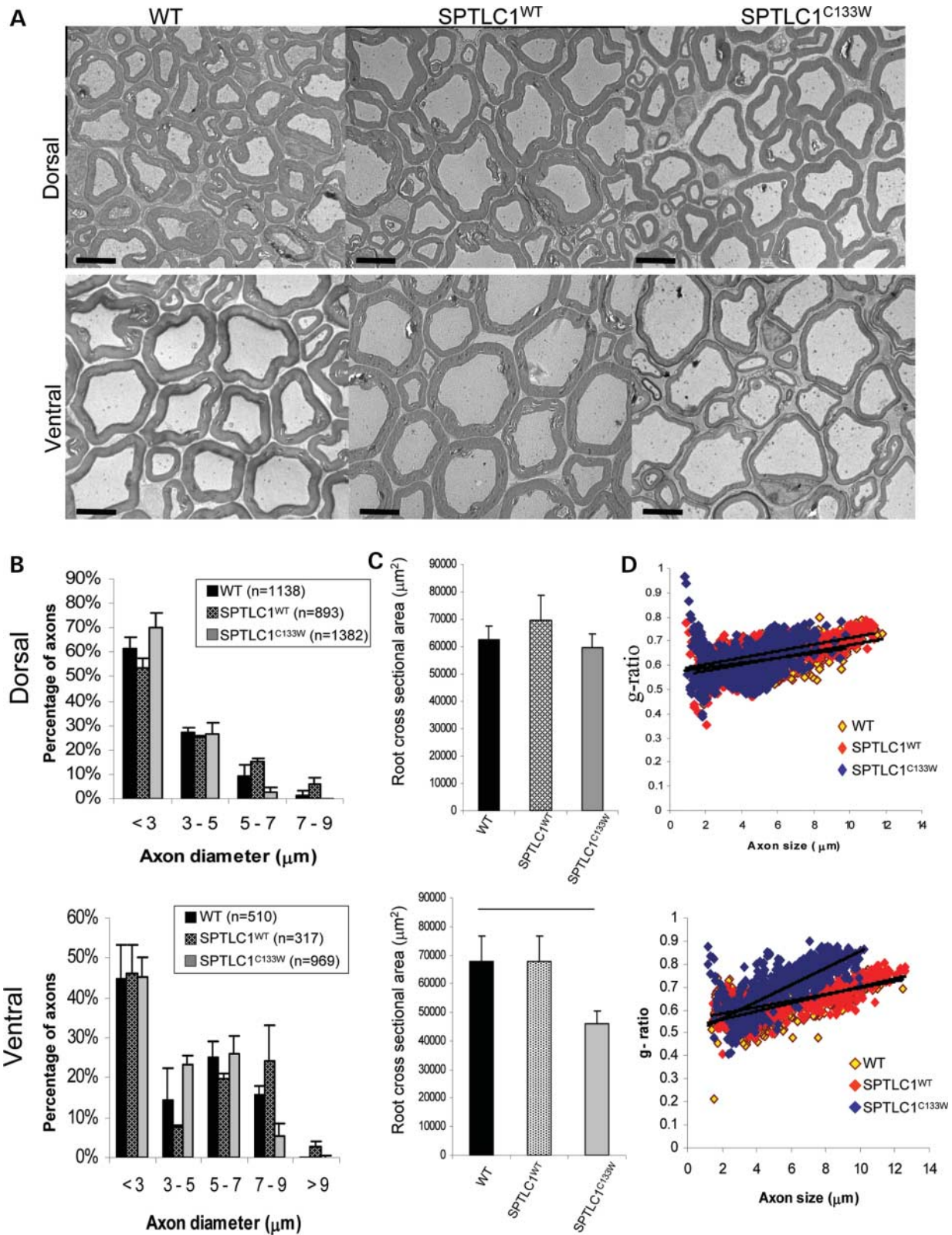
Figure 5. C133W mice have loss of large axons and myelin thinning in the ventral roots of the lumbar spinal cord. (**A**) Low power electron microscopic images of the dorsal and ventral roots from 10-month-oldwild-type, SPTLC1[WT] and SPTLC1[C133W] mice (bar = 4 µm). (**B**) Histogram of axon diameter distribution of axons in the dorsal and ventral roots. There is a loss of large axons from both tissues in the SPTLC1[C133W] mice. (**C**) Decreased cross-sectional area of the ventral root in SPTLC1[C133W] mice (*$P < 0.05$). (**D**) Myelin thinning of SPTLC1[C133W] axons in the ventral roots. *g*-ratio is plotted relative to the axon diameter with the best fit, linear regression indicated for each of the mice.
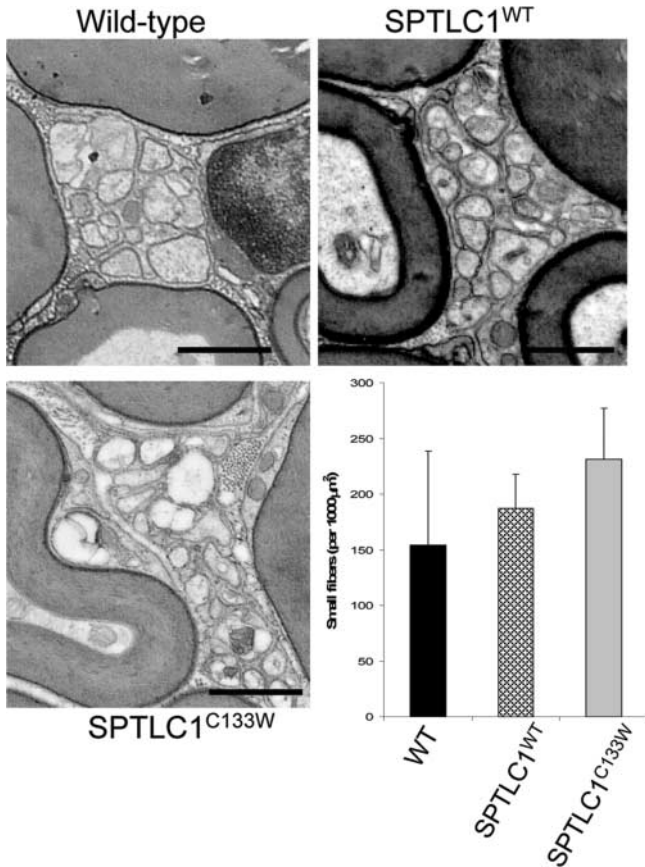
Figure 6. Preservation of small unmyelinated fibers in dorsal roots. (**A**) EM images of dorsal root axons from 10-month-old wild-type, SPTLC1[Tg-WT] and SPTLC1[C133W] mice. Small unmyelinated fibers are seen in all three conditions. The number of unmyelinated fibers per 1000 μm² is unchanged across conditions.

heavy chain (NFH), is used to detect axonal spheroids, which would reflect ongoing axonal degeneration within the spinal cord. We found no evidence of this type of degeneration. However, the staining pattern in the SPTLC1[C133W] mice was different from that in the SPTLC1[WT] mice. Neuronal bodies were clearly stained in all the sections taken from WT, SPTLC1[WT] and SPTLC1[C133W] mice. In contrast, the transversely cut axons were SMI32-positive only in the WT and SPTLC1[WT] lines; sections from the SPTLC1[C133W] mice did not stain with SMI32. When adjacent sections were probed with the SMI34, which recognizes phosphorylated NFH epitopes, staining was comparable between the SPTLC1[WT] and SPTLC1[C133W] mice. This suggests a change in the NFH phosphorylation state of the central axons of the SPTCL1[C133W] mice. However, as noted earlier, the absence of axonal spheroids suggests that axonal integrity is still largely preserved in these mice. It is worth noting that axonal spheroids have not been observed in HSAN1 patient tissue (23).

We next examined the DRG, assessing the overall appearance and the impact of transgene expression on specific neuronal subpopulations. Neuronal subpopulations in the DRG can be subclassified by histological stains and electrophysiological properties. The large neurons respond to proprioceptive and tactile signals and stain for neurofilament light chain (NFL) (24–26). The small neurons can be subdivided into NGF responsive, peptidergic, TrkA-positive (27–29) and GDNF-responsive, non-peptidergic and IB4-positive (30,31) populations. Both the TrkA and IB4-positive populations are involved in nociceptive responses, including thermal pain, and both give rise to the small myelinated and unmyelinated fibers (Aδ and C-fibers).

The gross appearance of the DRG by H&E staining was unremarkable, with no evidence of overt degeneration (Fig. 7A). Indeed, size estimations based on the number of 10 μm sections containing cell bodies also suggested that there was no overt decrease in DRG volume (data not shown). Transgene expression was confirmed in the DRG by immunofluorescence (Fig. 7B). The intensity of the transgene staining was markedly stronger in the SPTLC1[WT] DRGs. The transgene was expressed in NFL-positive and IB4-positive cells in both the SPTLC1[WT] and SPTLC1[C133W] mice (Fig. 6B). We quantified the number of IB4, TrkA and NFL-positive cells in the L4 DRGs from WT, SPTLC1[WT] and two different SPTLC1[C133W] lines (8B and 8E). Although there was no change in the number of NFL- and TrkA-positive cells, there was a significant decrease in the number of IB4-positive cells in the high expressing SPTLC1[C133W] mice (Fig. 7C). To confirm this change in cell distribution, we scored a separate group of L4 DRG neurons for expression of P2X₃, an ATP receptor expressed primarily in IB4-positive cells (28,32). P2X₃ immunostaining was also significantly decreased (data not shown).

IB4 and P2X₃ staining rapidly decreases after axonal damage (33,34); however, the neuronal soma can persist. Furthermore, axonal injury induces expression of activating transcription factor 3 (ATF3) (35,36), a member of the cAMP-response element binding protein transcription factor family (37). As such, it can be a useful marker for neurons with injured axons. We stained DRG sections from L3 for ATF3, NFL or IB4. ATF3-postive cells were present in low levels in the WT, SPTLC1[WT] and SPTLC1[C133W] tissues (Fig. 7D). Costaining of ATF3 with both IB4- and NFL-positive cells was observed, although in all conditions ATF3 colabeled more NFL- than IB4-positive cells. We quantified the number of cells staining positive with ATF3, NFL and IB4. Prior reports have focused on young mice and reported few to no ATF3-positive cells in naïve mice. We found that at 10 months of age, ~2% of wild-type DRG cells express ATF3 (Fig. 7E). Most of those cells were also NFL-positive. This may represent a normal aging process in mice. In the SPTLC1[C133W] DRG, roughly 6% of cells are ATF3-positive, with the majority of these cells costaining for NFL. The number of ATF-positive cells is less than typically seen in acute injury models; however, the results support the presence of chronic axonal injury in the SPTLC1[C133W] mice.

DISCUSSION

Expression of mutant SPTLC1 (SPTLC1[C133W]) in mice results in an age-dependent degeneration in multiple tissues that recapitulates several of the hallmark biochemical, behavioral
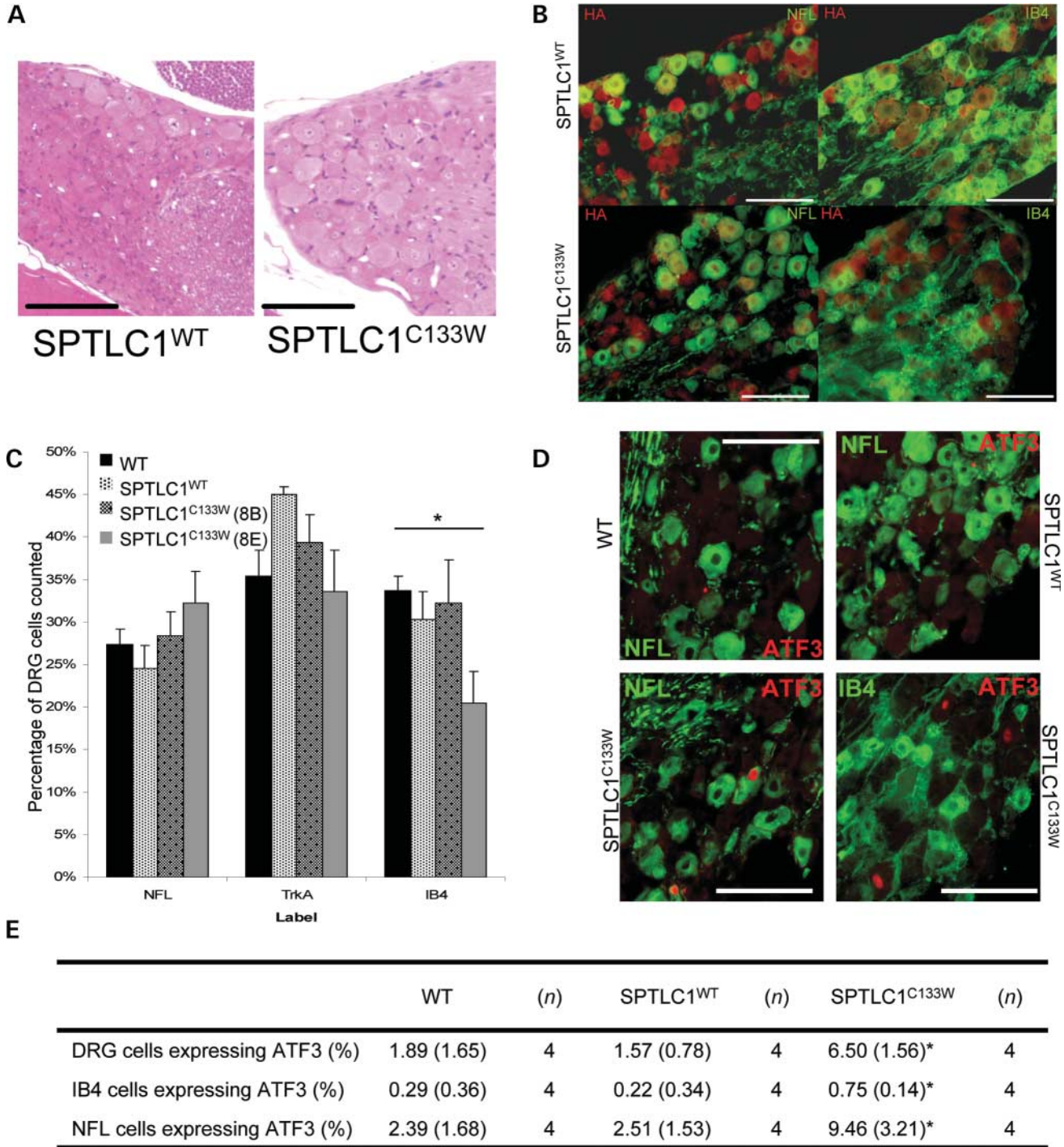
Figure 7. Diminished IB4- and increased ATF3-positive staining in the dorsal root ganglia of SPTLC1[C133W] mice. (**A**) H&E stain of DRG from SPTLC1[WT] and SPTLC1[C133W] mice (bar = 250 μm). (**B**) Colocalization of transgene with neurofilament light chain and IB4-positive cells in the DRG. (**C**) Decrease in the proportion of IB4-positive cells in the C133W-8E mouse ($P < 0.05$). There is ~30% decrease in the IB4-positive cell population. (**D**) Increased ATF3 staining in SPTLC1[C133W] DRG neurons. Background staining is present in WT and STPLC1[Tg-WT] cells. Preferential labeling with ATF3 in nuclei NFL-positive cells (lower left panel) versus IB4-postive cells (lower right panel). (**E**) Overall increase of ATF3 staining in SPTLC1[C133W] DRG. The number of cells colabeled with ATF3 and NFL or IB4 were tallied in L3 DRG. There was an increase in total ATF3 staining and in both the NFL and IB4 populations (*$P < 0.5$).

and histological changes in HSAN1. In the transgenic SPTLC1[C133W] mice, SPT activity is decreased in the liver and brain. This is consistent with reports of a dominant negative influence of mutant SPTLC1 in *in vitro* models and HSAN1 patient cells. In addition, the mutant mice developed altered motor, sensory and enteric performance, with most striking deficits in small sensory fiber and alimentary nerve functions. This also parallels the phenotype in HSAN1 in

which, in general, small fiber sensory loss is the predominant finding; motor and autonomic dysfunction are present, but are less severe. Furthermore, the SPTLC1^{C133W} mice show loss of large fibers in the dorsal and ventral roots, along with alterations in myelination in ventral roots. The DRG are reasonably preserved in the mice at 10 months. However, there are signs of peripheral stress, including loss of IB4 staining and increase in ATF3 staining. The overall neurological involvement appears less severe than the advanced stages of the disease in patients.

The neuronal pathology in the SPTLC1^{C133W} mice includes preferential loss of IB4 and P2X$_3$ staining in the DRG. The loss of signal is coupled with an increase in ATF3 expression, a marker for neuronal injury. In other models of peripheral nerve damage, loss of IB4 and P2X$_3$ staining is rapid, whereas residual cells up-regulate ATF3 expression (38). We detected ATF3 expression in both NFL-positive and NFL-negative cells in the DRG of SPTLC1^{C133W} mice. ATF3 expression in the NFL-positive cells is consistent with the loss of large axons in the dorsal roots. In addition, the presence of ATF3-positive, NFL-negative cells suggests peripheral damage in nociceptive neurons. The cell loss present in patients by end stage of the disease is more dramatic, with significant loss of the small cell population. The histological subclassification of the lost neurons in HSAN1 is unknown.

The sensitivity of sensory neurons to thermal pain appears to be regulated at the molecular level in part by changes in neuronal excitability or receptor expression. In normal mice, sensitivity to thermal pain decreases with age (39). In contrast, the SPTLC1^{C133W} mice show enhanced thermal sensitivity with age. The age-dependent changes in normal mice include decreased expression of voltage-gated sodium channel 1.8 (Na$_V$1.8) and thermosensitive ion channel receptor (TRP) expression. It will be interesting to see if these proteins change expression in the SPTLC1^{C133W} mice and to compare the time course with the thermal hyperalgesia.

One feature of HSAN1 not recapitulated in the mice is the ulcerative-mutilation of the extremities. We note that this feature is also lacking in some other mouse models of sensory loss such as that induced by expression of mutant Erb2, which leads to loss of Schwann cell myelination and selective loss of DRG neurons (40). This suggests that mice may be less prone than humans to digital ulceration after loss of pain sensation. The rat mutilated foot (mf) line has distal digit loss, which is reminiscent of the distal mutilations found in HSANs (41). The genetic lesion in the mf rat is a recessive, loss-of-function mutation in the cystosolic chaperonin-containing t-complex, peptide-1 (Cct4) gene (42). These rats have near-complete denervation of the hind foot epidermis by day P7, accompanied by elevated pain thresholds (43). Mice null for the TrkA receptor have near-complete denervation of the skin, along with a loss of nociceptive neurons and sympathetic chain ganglia neurons (44). These mice develop skin lesions and foot mutilations, suggesting that foot mutilation may only manifest in mice in the absence of TrkA-positive, nociceptive neurons. The severity of the mutation leads to death within 2–3 weeks. Interestingly, human HSAN IV is caused by loss of function mutations in TrkA (45). Human HSAN IV does not have ulcerative mutilations

associated with it; however, there is a profound sensory loss accompanied with loss of epidermal small fiber innervation (23). Thus, it is unclear what the necessary prerequisites are for ulcerative mutilations. Indeed, there is evidence that SPT is upregulated in keratinocytes in response to UVB damage (46). This has led to speculation that alterations in skin sphingolipid may exacerbate injuries resulting from lack of sensory feedback (13).

The origin of the exocrine pancreatic degeneration is unclear. Grossly evident pancreatic degeneration has not been reported in HSAN1 patients or in more severe cases of autonomic dysfunctions. In humans, the leading cause of exocrine pancreatic degeneration is obstruction of the common duct by gallstones (47), leading to premature activation of pancreatic digestive enzymes and acinar cell death. Biliary obstruction with secondary pancreatic degeneration is usually associated with pancreatitis in humans. This would be expected to have inflammation as well as tissue saponification with calcification. None of these changes are seen in these mice. The early advent of the pancreatic degeneration raises the issue as to whether it is a developmental or degenerative process. The divergence of pancreatic degeneration phenotype between humans and mice may reflect different physiologies, differences in the expression pattern of the transgene when compared with the endogenous gene, or some other property of the transgene construct.

Expression of SPTLC1^{C133W} induces pathology in a number of tissues in the SPTLC1^{C133W} mice, although the mechanism for this toxicity is unclear. The pathology may result from a reduction in SPT activity, an unrelated adverse toxic property of the mutant protein, or a combination of both. A common mechanism for neurodegeneration in humans is the toxic accumulation of misfolded proteins (48). Evidence implicates a role for such a mechanism in amyotrophic lateral sclerosis, the polyglutamine diseases, Parkinson disease and Alzheimer disease. In each of these diseases, histological studies demonstrate the presence of insoluble protein aggregates or inclusion bodies in both neuronal and non-neuronal cells. We have found no indication for such protein structures in our mice or in transient transfection of the constructs. These data are consistent with the hypothesis that pathology in the SPTLC1^{C133W} mice is a consequence of the loss of SPT activity.

The expression of mutant SPTLC1 appears to a have paradoxical effect on ceramide levels. SPT is the key enzyme of *de novo* ceramide synthesis (49,50) and is essential for complex sphingolipid synthesis; one may therefore anticipate that a reduction in SPT activity would result in a loss of total ceramide. In contrast, our SPTLC1^{C133W} mice have decreased SPT activity, but show no reduction in total ceramide levels. This may reflect a set of compensatory adaptations which are required to sustain viability. Also unexpected is the observed increase in long chain ceramides (C16:0 and C18:0), a subset of the pool of total ceramides. Two points are noted here. First, these ceramides are precursors of glucosylceramide, previously reported to be elevated in HSAN1 (5). Secondly, although the mechanism for elevation of these ceramides is not clear, it may reflect a subtle increase in the availability of palmitic acid because of reduced SPT activity.

The increased levels of C16:0 and C18:0 ceramides could play a role in the degeneration of axons and neurons in the SPTLC1^{C133W} mice, as an analogous increase in levels of these ceramides is detected in neurons in the spinal cords of ALS patients and in the brains of Alzheimer's disease and HIV dementia patients (51–53). Studies of cell culture and mouse models in the later studies provided evidence that the ceramides may mediate the dysfunction and death of neurons in these neurodegenerative disorders. Further work will be necessary to understand the relationship, if any, between the biochemical changes and the pathology.

Why mutations in SPT result in phenotypes in humans and mice with prominent involvement of small sensory neurons remains unexplained. Conceivably, the affected neuronal populations have an increased requirement for sphingolipid synthesis. This is consistent with the observation that a second dominantly inherited, hereditary sensory neuropathy with ulcerative mutilations, Charcot–Marie–Tooth (Type 2B) (CMT2B), is caused by Rab7 mutations (54,55). Rab7 is found in the late endosome and seems to have a role in sphingolipid recycling (56). The fact that there are two phenotypically similar diseases, both with mutations that disrupt sphingolipid metabolism, supports the biochemical-defect hypothesis for HSAN1. Ultimately, to demonstrate that the disease process is caused by the loss of SPT activity, and not by toxicity of the mutant SPTLC1 protein, will require dissociation of the reduced SPT activity from expression of the mutant protein. This would allow for testing the correlation between levels of SPT activity and the emergence of a neuronal phenotype.

MATERIALS AND METHODS

Transgene construction and generation of transgenic mice

C. Griseus cDNA for the SPTLC1 gene was subcloned into a pcDNA3.1 vector between the *Eco*RI and *Xba*I sites. The *Xba*I site was eliminated by redigestion with *Xba*I and filled in with Klenow fragment. Novel *Xba*I and *Avr*II sites were introduced on either side of the stop codon by quick change mutagenesis (QCM). For the tagged constructs, the *Spe*I-ended triple-HA cassettes were ligated into the *Xba*I site preceding the stop codon. The tagged and untagged genes were subjected to QCM to introduce the C133W mutation using primers designed to eliminate the neighboring *Kpn*I site without altering the amino acids encoded. The four *Eco*RI to *Avr*II cassettes were moved from the pCDNA3.1 vector to the modified pCAGGS vector. The pCAGGS vector was modified by QCM to eliminate the downstream *Eco*RI site and to introduce both a *Kpn*I and an *Nhe*I site between *Xho*I and *Bgl*II sites.

The final transgene construct consists of the chicken beta-actin promoter with CMV immediate early gene enhancer elements, actin, followed by the SPTLC1 cDNA with HA, and the rabbit β-globin poly-adenylation signal. The 3.7 kb transgene was isolated from the plasmid by a *Hin*dIII/*Pvu*II digest for microinjection. Mice were generated with standard techniques in the BL6/C3H background. Presence of the transgene was detected by PCR amplification of genomic DNA extracted with the DNeasy Tissue Extraction kit (Qiagen, Valencia,CA, USA). Multiplex PCR was completed with primers for the transgene (F, 5′-CGAAAAACCATCCTG-CTCTC-3′; R, 5′-GGACAGACGGTTCCAGTGTT-3′) and an endogenous locus, the ABCD1 gene (F, 5′-GAGG-GAGGTGGAAGGAAAGA-3′; R. 5′-GAAGGGTTGTTGCT-CTGACC-3′).

Cell culture and transfection

CHO-K1 cells, maintained in Dulbecco's Modified Eagles Medium (Mediatech, Herndon, VA, USA) containing 10% fetal bovine serum (JRH Biosciences, Lenexa, KS, USA), were transfected using Lipofectamine 2000 (Invitrogen, Carlsbad, CA, USA), as previously described (57).

SPT assay

A reaction cocktail containing final concentrations of 0.1 M HEPES (pH 8.3), 5 mM DTT, 1 mM serine (10 µC/ml [^{3}H]-serine), 1 mM NADPH, 1 mM NADH, 50 µM pydridoxal-5′-phosphate, membrane protein (0.1–0.2 mg/ml) and palmitoyl-CoA (0.025–0.05 mM) was reacted at 37°C for 10 min. The reaction was started by the addition of CoA and protein. After the 10 min reaction time, NH$_4$OH to a final 0.25 M was added, followed by the addition of 1.5 ml of CHCl$_3$:methanol (1:2), and vortexed. Long chain bases were extracted by adding 1 ml CHCl$_3$ and 2 ml of 0.5 M NH$_4$OH, vortexing and centrifuging briefly. The upper aqueous layer was aspirated off and the lower layer was washed with 2 ml of 30 mM KCl and centrifuged. The washing was carried out three times. One milliliter of the sample was dried and counted.

Western blotting

Microsomal membranes. Perfused tissue was Potter-homogenized in membrane buffer (50 mM Tris, pH 7.5, 1 mM EGTA, 1 mM βME, 1 mM PMSF, 1 µg/ml leupeptin, pepstatin A and aprotinin) and spun at 15 000g for 20 min to remove cell debris and mitochondria. The supernatant was spun at 100 000g for 30 min, generously resuspended in membrane buffer and pelleted at 100 000g. The resulting pellet was resuspended in membrane buffer containing 33% glycerol and frozen at −80°C.

Mouse tissue. Mice were perfused with 50 ml of 0.9% NaCl with a transcardial perfusion. After dissection, tissue was snap-frozen with liquid nitrogen. Tissue was placed in homogenization buffer (10 mM MOPS, pH 7.4, 0.25% Triton X-100) in the presence of complete protease inhibitor tablets (Roche, Indianapolis, IN, USA) and homogenized with a polytron blade. The lysate was spun at 1000g at 4°C for 5 min. The resulting supernatant was homogenized with six strokes of a Potter–Elvehjem homogenizer and spun at 15 000g for 10 min at 4°C. Protein concentration was determined by Coomassie assay and lysates were separated by standard western blotting techniques. Membranes were probed with anti-LCB1 (BD Pharmigen, San Diego, CA, USA), HRP-conjugated anti-HA (Roche) or anti-actin (Sigma, St Louis, MO, USA). SPTLC2 antibodies were generated by

SigmaGenosys (The Woodlands, TX, USA) using a combination of peptides (CGKYSRHRLVPLLDRPF, amino acids 538–552 and CGDRPFDETTYEETED, amino acids 549–561) and subsequently affinity-purified versus the peptides. Primary antibodies were detected with the appropriate HRP-conjugated secondary antibody (Jackson ImmunoResearch, West Grove, PA, USA) and visualized with ECL Plus (Amersham, Piscataway, NJ, USA).

Behavioral assays

Leg activity. Six-month-old mice were suspended by the tail and a 30 s video was recorded. Videos were evaluated in a blinded manner by experienced observers of tail lift tests. Hind limb activity was scored on a 10-point scale, with 1 indicating minimal leg motion and 10 indicating extreme leg hyperkinesis. Five animals per group condition were evaluated. Significant differences were assessed by Mann–Whitney test.

Motor function. Motor function was assessed by rotorod analysis in an accelerating rod paradigm. Mice were acclimated to the rotorod apparatus for 3 days. For use in the trial, the mouse must successfully remain on a steadily rotating rod for 1 min for three times. Each mouse was given five trials a day for 3 days to successfully meet the criteria. Eight mice per group successfully completed the trial. Latency to fall was measured as the rod speed was increased from 5 to 40 r.p.m. over 5 min. Each mouse was tested in three trials per day over 3 days. The mean latencies to fall were compared on each day by a one-way ANOVA. Mice were tested at 6 months and 10 months of age.

Sensory tests. Sensory performance was evaluated as previously described (58). Mice were tested at 6 months and 10 months of age. Statistical differences were assessed by Mann–Whitney (Von Frey and Pin Prick) or ANOVA (acetone and hot plate tests).

Lipid extraction and measurements of sphingolipids, phospholipids and lipid peroxides

Mice were perfused with 50 ml 0.9% saline and the spinal cord was removed and snap-frozen with liquid nitrogen. Total lipids from samples were prepared according to a modified Bligh and Dyer procedure (53). Briefly, each sample was homogenized at room temperature in 10 volumes of deionized water, then in three volumes of 100% methanol containing 30 mmol/l ammonium formate and vortexed. Four volumes of chloroform was added, and the mixture was vortexed and centrifuged at $1000g$ for 10 min. The bottom (chloroform) layer was removed and analyzed by direct injection into a Sciex 3000 tandem mass spectrometer. Electro-spray ionization tandem mass spectrometry (ESI/MS/MS) analyses were performed using methods similar to those used in our previous studies (53). Samples were injected for 3 min, allowing for accumulation of mass counts, and the sum of the total counts under each peak was used to quantify each species relative to a standard curve. Sphingomyelin and ceramide standards C16:0 and C18:0 were purchased from Sigma, as were the standards for cholesterol and the cholesterol esters C16:0 and C18:0. Ceramides C20:0 and C24:0, palmitoyl–lactosyl ceramide C16:0–C16:0, stearoyl–lactosyl–ceramide C16:0–C18:0, lignoceryl–glucosyl–ceramide C16:0–C24:0, lignoceryl–galactosyl–ceramide C16:0–C24:0 and stearoyl–galactosyl–ceramide–sulfate C18:1–C24:0 were purchased from Matreya Inc. (Pleasant Gap, PA, USA).

Histology

Whole mouse pathology. Mice at 4 months and 10 months of age were anesthetized, followed by transcardial perfusion with 0.9% saline and then with Bouin's solution. Whole mouse was post-fixed for 2 weeks at 4°C in Bouin's solution. Paraffin-embedded sections were cut at 4 μm and stained with H&E, Luxol fast blue or silver stain. Immunohistochemistry for PGP9.5 in pancreatic sections was completed using standard techniques. Briefly, sections were dewaxed and antigen retrieval was done by boiling in 10 mM citrate buffer. After hydration, sections were probed with anti-PGP9.5 (Biogenesis, Kingston, NH, USA), followed by biotinylated anti-rabbit secondary. Staining was visualized with an ABC kit and SG Chromagen substrate (Vector Laboratories, Burlingame, CA, USA).

Electron microscopy

Mice at 10 months of age were perfused with 3% formaldehyde and 3% glutaraldehyde. Ventral and dorsal roots of the spinal cord from the lumbar region were dissected out and post-fixed in 2.5% glutaraldehyde overnight. Roots were osmificated with 1% osmium tetroxide and embedded in an araldite resin. For axon distribution and *g*-ratio calculations, four random non-overlapping regions were imaged at 2500× magnification of three different roots from each condition. Axon size and fiber size were calculated using ImageJ. For small fiber densities, eight non-overlapping images from three roots for each condition were imaged at 10 000× magnification. The total number of fibers was counted and fiber density calculated. Statistical significance was determined by a *t*-test.

Immunofluorescence

Spinal cord and dorsal root ganglia from the lumber region were dissected from 10-month-old mice perfused with 4% paraformaldehyde. Tissue was post-fixed overnight at 4°C in paraformaldehyde and then transferred to 30% sucrose. Tissue was embedded in OCT and cut into 10 μm sections. For DRG cell counts, every fourth section was taken. Tissues were blocked so that all four conditions were cut on to the same slide to ensure equivalent processing of samples. DRGs were stained with rabbit anti-HA (Abcam, Cambridge, MA, USA), mouse anti-NFL (Sigma), anti-TrkA (Upstate Biotechnology, Waltham, MA, USA), anti-P2X$_3$ (Chemicon, Temecula, CA, USA), anti-ATF3 (Santa Cruz Biotechnology, Santa Cruz, CA, USA) or biotinylated isolectin IB4 (Sigma). Cell counts were done on the bilateral L4 DRGs from three animals per condition.

ACKNOWLEDGEMENTS

SUPPLEMENTARY MATERIAL

Supplementary Material is available at HMG Online.

REFERENCES

1. Auer-Grumbach, M., De Jonghe, P., Verhoeven, K., Timmerman, V., Wagner, K., Hartung, H.P. and Nicholson, G.A. (2003) Autosomal dominant inherited neuropathies with prominent sensory loss and mutilations: a review. *Arch. Neurol.*, **60**, 329–334.
2. Dyck, P.J., Lambert, E.H. and Nichols, P.C. (1971) Quantitative measurement of sensation related to compound action potential and number and sizes of myelinated and unmyelinated fibers of sural nerve in health, Friedreich ataxia, hereditary sensory neuropathy, and tabes dorsalis. In Cobb, W. (ed.), *Handbook of Electroencephalography and Clinical Neurophysiology.* Elsevier, Amsterdam, Vol. 9.
3. Denny-Brown, D. (1951) Hereditary sensory radicular neuropathy. *J. Neurochem.*, **14**, 237–252.
4. Brock, S. (1953) *The Basis of Clinical Neurology: the Anatomy and Physiology of the Nervous System in Their Application to Clinical Neurology.* 3rd ed. Williams and Wilkins, Baltimore.
5. Dawkins, J.L., Hulme, D.J., Brahmbhatt, S.B., Auer-Grumbach, M. and Nicholson, G.A. (2001) Mutations in SPTLC1, encoding serine palmitoyltransferase, long chain base subunit-1, cause hereditary sensory neuropathy type I. *Nat. Genet.*, **27**, 309–312.
6. Bejaoui, K., Wu, C., Scheffler, M.D., Haan, G., Ashby, P., Wu, L., de Jong, P. and Brown, R.H., Jr (2001) SPTLC1 is mutated in hereditary sensory neuropathy, type 1. *Nat. Genet.*, **27**, 261–262.
7. Gable, K., Han, G., Monaghan, E., Bacikova, D., Natarajan, M., Williams, R. and Dunn, T.M. (2002) Mutations in the yeast LCB1 and LCB2 genes, including those corresponding to the hereditary sensory neuropathy type I mutations, dominantly inactivate serine palmitoyltransferase. *J. Biol. Chem.*, **277**, 10 194–10 200.
8. Hannun, Y.A. and Luberto, C. (2000) Ceramide in the eukaryotic stress response. *Trends Cell Biol.*, **10**, 73–80.
9. Venkataraman, K. and Futerman, A.H. (2000) Ceramide as a second messenger: sticky solutions to sticky problems. *Trends Cell Biol.*, **10**, 408–412.
10. Cremesti, A., Paris, F., Grassme, H., Holler, N., Tschopp, J., Fuks, Z., Gulbins, E. and Kolesnick, R. (2001) Ceramide enables fas to cap and kill. *J. Biol. Chem.*, **276**, 23 954–23 961.
11. van Blitterswijk, W.J., van der Luit, A.H., Veldman, R.J., Verheij, M. and Borst, J. (2003) Ceramide: second messenger or modulator of membrane structure and dynamics? *Biochem. J.*, **369**, 199–211.
12. Verhoeven, K., Coen, K., De Vriendt, E., Jacobs, A., Van Gerwen, V., Smouts, I., Pou-Serradell, A., Martin, J.J., Timmerman, V. and De Jonghe, P. (2004) SPTLC1 mutation in twin sisters with hereditary sensory neuropathy type I. *Neurology*, **62**, 1001–1002.
13. Bejaoui, K., Uchida, Y., Yasuda, S., Ho, M., Nishijima, M., Brown, R.H., Jr, Holleran, W.M. and Hanada, K. (2002) Hereditary sensory neuropathy type 1 mutations confer dominant negative effects on serine palmitoyltransferase, critical for sphingolipid synthesis. *J. Clin. Invest.*, **110**, 1301–1308.

14. Dawkins, J.L., Brahmbhatt, S., Auer-Grumbach, M., Wagner, K., Hartung, H.P., Verhoeven, K., Timmerman, V., De Jonghe, P., Kennerson, M., LeGuern, E. *et al.* (2002) Exclusion of serine palmitoyltransferase long chain base subunit 2 (SPTLC2) as a common cause for hereditary sensory neuropathy. *Neuromuscul. Disord.*, **12**, 656–658.
15. Dedov, V.N., Dedova, I.V., Merrill, A.H., Jr and Nicholson, G.A. (2004) Activity of partially inhibited serine palmitoyltransferase is sufficient for normal sphingolipid metabolism and viability of HSN1 patient cells. *Biochim. Biophys. Acta*, **1688**, 168–175.
16. Bossy-Wetzel, E., Schwarzenbacher, R. and Lipton, S.A. (2004) Molecular pathways to neurodegeneration. *Nat. Med.*, **10** (suppl.), S2–S9.
17. Hanada, K., Hara, T., Nishijima, M., Kuge, O., Dickson, R.C. and Nagiec, M.M. (1997) A mammalian homolog of the yeast LCB1 encodes a component of serine palmitoyltransferase, the enzyme catalyzing the first step in sphingolipid synthesis. *J. Biol. Chem.*, **272**, 32 108–32 114.
18. Su, A.I., Cooke, M.P., Ching, K.A., Hakak, Y., Walker, J.R., Wiltshire, T., Orth, A.P., Vega, R.G., Sapinoso, L.M., Moqrich, A. *et al.* (2002) Large-scale analysis of the human and mouse transcriptomes. *Proc. Natl Acad. Sci. USA*, **99**, 4465–4470.
19. Boorman, G.A. and Sills, R.C. (1999) *Pathology of the Mouse.* Cache River Press, Vienna, IL, USA.
20. Rossi, J., Herzig, K.H., Voikar, V., Hiltunen, P.H., Segerstrale, M. and Airaksinen, M.S. (2003) Alimentary tract innervation deficits and dysfunction in mice lacking GDNF family receptor alpha2. *J. Clin. Invest.*, **112**, 707–716.
21. Tezel, E., Hibi, K., Nagasaka, T. and Nakao, A. (2000) PGP9.5 as a prognostic factor in pancreatic cancer. *Clin. Cancer Res.*, **6**, 4764–4767.
22. Vernino, S., Ermilov, L.G., Sha, L., Szurszewski, J.H., Low, P.A. and Lennon, V.A. (2004) Passive transfer of autoimmune autonomic neuropathy to mice. *J. Neurosci.*, **24**, 7037–7042.
23. Klein, C.J. and Dyck, P.J. (2005) HSANs: clinical features, patholgic classification, and molecular genetics. In Dyck, P.J. and Thomas, P.K. (eds), *Peripheral Neuropathy.* 4th ed. W.B. Saunders, Philadelphia, PA, Vol. 2, pp. 1809–1844.
24. Price, J. (1985) An immunohistochemical and quantitative examination of dorsal root ganglion neuronal subpopulations. *J. Neurosci.*, **5**, 2051–2059.
25. Lawson, S.N. and Waddell, P.J. (1991) Soma neurofilament immunoreactivity is related to cell size and fibre conduction velocity in rat primary sensory neurons. *J. Physiol.*, **435**, 41–63.
26. Lawson, S.N., Perry, M.J., Prabhakar, E. and McCarthy, P.W. (1993) Primary sensory neurones: neurofilament, neuropeptides, and conduction velocity. *Brain Res. Bull.*, **30**, 239–243.
27. McMahon, S.B., Armanini, M.P., Ling, L.H. and Phillips, H.S. (1994) Expression and coexpression of Trk receptors in subpopulations of adult primary sensory neurons projecting to identified peripheral targets. *Neuron*, **12**, 1161–1171.
28. Averill, S., McMahon, S.B., Clary, D.O., Reichardt, L.F. and Priestley, J.V. (1995) Immunocytochemical localization of trkA receptors in chemically identified subgroups of adult rat sensory neurons. *Eur. J. Neurosci.*, **7**, 1484–1494.
29. Molliver, D.C., Radeke, M.J., Feinstein, S.C. and Snider, W.D. (1995) Presence or absence of TrkA protein distinguishes subsets of small sensory neurons with unique cytochemical characteristics and dorsal horn projections. *J. Comp. Neurol.*, **361**, 404–416.
30. Plenderleith, M.B., Cameron, A.A., Key, B. and Snow, P.J. (1988) Soybean agglutinin binds to a subpopulation of primary sensory neurones in the cat. *Neurosci. Lett.*, **86**, 257–262.
31. Plenderleith, M.B. and Snow, P.J. (1993) The plant lectin Bandeiraea simplicifolia I-B4 identifies a subpopulation of small diameter primary sensory neurones which innervate the skin in the rat. *Neurosci. Lett.*, **159**, 17–20.
32. Snider, W.D. and McMahon, S.B. (1998) Tackling pain at the source: new ideas about nociceptors. *Neuron*, **20**, 629–632.
33. Averill, S., Michael, G.J., Shortland, P.J., Leavesley, R.C., King, V.R., Bradbury, E.J., McMahon, S.B. and Priestley, J.V. (2004) NGF and GDNF ameliorate the increase in ATF3 expression which occurs in dorsal root ganglion cells in response to peripheral nerve injury. *Eur. J. Neurosci.*, **19**, 1437–1445.
34. Bradbury, E.J., Burnstock, G. and McMahon, S.B. (1998) The expression of P2X3 purinoreceptors in sensory neurons: effects of axotomy and glial-derived neurotrophic factor. *Mol. Cell. Neurosci.*, **12**, 256–268.
35. Tsuzuki, K., Kondo, E., Fukuoka, T., Yi, D., Tsujino, H., Sakagami, M. and Noguchi, K. (2001) Differential regulation of P2X(3) mRNA

expression by peripheral nerve injury in intact and injured neurons in the rat sensory ganglia. *Pain*, **91**, 351–360.

36. Tsujino, H., Kondo, E., Fukuoka, T., Dai, Y., Tokunaga, A., Miki, K., Yonenobu, K., Ochi, T. and Noguchi, K. (2000) Activating transcription factor 3 (ATF3) induction by axotomy in sensory and motoneurons: a novel neuronal marker of nerve injury. *Mol. Cell. Neurosci.*, **15**, 170–182.
37. Hai, T.W., Liu, F., Coukos, W.J. and Green, M.R. (1989) Transcription factor ATF cDNA clones: an extensive family of leucine zipper proteins able to selectively form DNA-binding heterodimers. *Genes Dev.*, **3**, 2083–2090.
38. Wang, R., Guo, W., Ossipov, M.H., Vanderah, T.W., Porreca, F. and Lai, J. (2003) Glial cell line-derived neurotrophic factor normalizes neurochemical changes in injured dorsal root ganglion neurons and prevents the expression of experimental neuropathic pain. *Neuroscience*, **121**, 815–824.
39. Wang, S., Davis, B.M., Zwick, M., Waxman, S.G. and Albers, K.M. (2005) Reduced thermal sensitivity and Nav1.8 and TRPV1 channel expression in sensory neurons of aged mice. *Neurobiol. Aging*.
40. Chen, S., Rio, C., Ji, R.R., Dikkes, P., Coggeshall, R.E., Woolf, C.J. and Corfas, G. (2003) Disruption of ErbB receptor signaling in adult non-myelinating Schwann cells causes progressive sensory loss. *Nat. Neurosci.*, **6**, 1186–1193.
41. Jacobs, J.M., Scaravilli, F., Duchen, L.W. and Mertin, J. (1981) A new neurological rat mutant 'mutilated foot'. *J. Anat.*, **132**, 525–543.
42. Lee, M.J., Stephenson, D.A., Groves, M.J., Sweeney, M.G., Davis, M.B., An, S.F., Houlden, H., Salih, M.A., Timmerman, V., de Jonghe, P. *et al.* (2003) Hereditary sensory neuropathy is caused by a mutation in the delta subunit of the cytosolic chaperonin-containing t-complex peptide-1 (Cct4) gene. *Hum. Mol. Genet.*, **12**, 1917–1925.
43. Hsu, S.H., Lee, M.J., Hsieh, S.C., Scaravilli, F. and Hsieh, S.T. (2004) Cutaneous and sympathetic denervation in neonatal rats with a mutation in the delta subunit of the cytosolic chaperonin-containing t-complex peptide-1 gene. *Neurobiol. Dis.*, **16**, 335–345.
44. Smeyne, R.J., Klein, R., Schnapp, A., Long, L.K., Bryant, S., Lewin, A., Lira, S.A. and Barbacid, M. (1994) Severe sensory and sympathetic neuropathies in mice carrying a disrupted Trk/NGF receptor gene. *Nature*, **368**, 246–249.
45. Indo, Y., Mardy, S., Miura, Y., Moosa, A., Ismail, E.A., Toscano, E., Andria, G., Pavone, V., Brown, D.L., Brooks, A. *et al.* (2001) Congenital insensitivity to pain with anhidrosis (CIPA): novel mutations of the TRKA (NTRK1) gene, a putative uniparental disomy, and a linkage of the mutant TRKA and PKLR genes in a family with CIPA and pyruvate kinase deficiency. *Hum. Mutat.*, **18**, 308–318.
46. Farrell, A.M., Uchida, Y., Nagiec, M.M., Harris, I.R., Dickson, R.C., Elias, P.M. and Holleran, W.M. (1998) UVB irradiation up-regulates serine palmitoyltransferase in cultured human keratinocytes. *J. Lipid Res.*, **39**, 2031–2038.
47. Lerch, M.M., Saluja, A.K., Runzi, M., Dawra, R., Saluja, M. and Steer, M.L. (1993) Pancreatic duct obstruction triggers acute necrotizing pancreatitis in the opossum. *Gastroenterology*, **104**, 853–861.
48. Rao, R.V. and Bredesen, D.E. (2004) Misfolded proteins, endoplasmic reticulum stress and neurodegeneration. *Curr. Opin. Cell Biol.*, **16**, 653–662.
49. Futerman, A.H. and Riezman, H. (2005) The ins and outs of sphingolipid synthesis. *Trends Cell Biol.*, **15**, 312–318.
50. Perry, D.K. (2002) Serine palmitoyltransferase: role in apoptotic *de novo* ceramide synthesis and other stress responses. *Biochim. Biophys. Acta*, **1585**, 146–152.
51. Cutler, R.G., Haughey, N.J., Tammara, A., McArthur, J.C., Nath, A., Reid, R., Vargas, D.L., Pardo, C.A. and Mattson, M.P. (2004) Dysregulation of sphingolipid and sterol metabolism by ApoE4 in HIV dementia. *Neurology*, **63**, 626–630.
52. Cutler, R.G., Kelly, J., Storie, K., Pedersen, W.A., Tammara, A., Hatanpaa, K., Troncoso, J.C. and Mattson, M.P. (2004) Involvement of oxidative stress-induced abnormalities in ceramide and cholesterol metabolism in brain aging and Alzheimer's disease. *Proc. Natl Acad. Sci. USA*, **101**, 2070–2075.
53. Cutler, R.G., Pedersen, W.A., Camandola, S., Rothstein, J.D. and Mattson, M.P. (2002) Evidence that accumulation of ceramides and cholesterol esters mediates oxidative stress-induced death of motor neurons in amyotrophic lateral sclerosis. *Ann. Neurol.*, **52**, 448–457.
54. Houlden, H., King, R.H., Muddle, J.R., Warner, T.T., Reilly, M.M., Orrell, R.W. and Ginsberg, L. (2004) A novel RAB7 mutation associated with ulcero-mutilating neuropathy. *Ann. Neurol.*, **56**, 586–590.
55. Verhoeven, K., De Jonghe, P., Coen, K., Verpoorten, N., Auer-Grumbach, M., Kwon, J.M., FitzPatrick, D., Schmedding, E., De Vriendt, E., Jacobs, A. *et al.* (2003) Mutations in the small GTP-ase late endosomal protein RAB7 cause Charcot–Marie–Tooth type 2B neuropathy. *Am. J. Hum. Genet.*, **72**, 722–727.
56. Choudhury, A., Sharma, D.K., Marks, D.L. and Pagano, R.E. (2004) Elevated endosomal cholesterol levels in Niemann–Pick cells inhibit rab4 and perturb membrane recycling. *Mol. Biol. Cell*, **15**, 4500–4511.
57. Han, G., Gable, K., Yan, L., Natarajan, M., Krishnamurthy, J., Gupta, S.D., Borovitskaya, A., Harmon, J.M. and Dunn, T.M. (2004) The topology of the Lcb1p subunit of yeast serine palmitoyltransferase. *J. Biol. Chem.*, **279**, 53707–53716.
58. Broom, D.C., Samad, T.A., Kohno, T., Tegeder, I., Geisslinger, G. and Woolf, C.J. (2004) Cyclooxygenase 2 expression in the spared nerve injury model of neuropathic pain. *Neuroscience*, **124**, 891–900.